Journal of Magnetic Resonance 221 (2012) 11–18

Contents lists available at SciVerse ScienceDirect

Journal of Magnetic Resonance

journal homepage: www.elsevier.com/locate/jmr

Characterizing permeability and stability of microcapsules for controlled drug delivery by dynamic NMR microscopy

Stefan Henning [a,*], Daniel Edelhoff [a], Benedikt Ernst [a], Sabine Leick [b], Heinz Rehage [b], Dieter Suter [a]

[a] Experimental Physics III, TU Dortmund University, 44227 Dortmund, Germany
[b] Physical Chemistry II, TU Dortmund University, 44227 Dortmund, Germany

ARTICLE INFO

Article history:
Received 22 February 2012
Revised 7 May 2012
Available online 26 May 2012

Keywords:
Imaging
Drug delivery
Microcapsules
Diffusion
Paramagnetic contrast agent

ABSTRACT

Microscopic capsules made from polysaccharides are used as carriers for drugs and food additives. Here, we use NMR microscopy to assess the permeability of capsule membranes and their stability under different environmental conditions. The results allow us to determine the suitability of different capsules for controlled drug delivery. As a measure of the membrane permeability, we monitor the diffusion of paramagnetic molecules into the microcapsules by dynamic NMR microimaging. We obtained the diffusion coefficients of the probe molecules in the membranes and in the capsule core by comparing the measured time dependent concentration maps with numerical solutions of the diffusion equation. The results reveal that external coatings strongly decrease the permeability of the capsules. In addition, we also visualized that the capsules are stable under gastric conditions but dissolve under simulated colonic conditions, as required for targeted drug delivery. Depending on the capsule, the timescales for these processes range from 1 to 28 h.

1. Introduction

Magnetic resonance imaging (MRI) of small samples with high resolution on the order of 10 μm is known as NMR microscopy (μMRI, MR microimaging) and has been shown to be an excellent tool for a large variety of non-invasive investigations in medicine, biology and material sciences [1,2]. Besides the investigations of static microscopic structures, NMR microscopy is especially powerful for probing dynamic processes like diffusion or flow. Such measurements of diffusion and flow are commonly achieved by using pulsed magnetic field gradients for encoding spatial information into a phase factor of a spin echo [3], leading to maps of apparent diffusion coefficients or velocities [4]. An alternative way of measuring diffusion processes relies on the utilization of magnetic resonance contrast agents (CA) which greatly enhance the sensitivity [5]. Paramagnetic molecules like chelates of the gadolinium ion, which enhance the relaxivity of surrounding molecules and therefore generate concentration depending signal amplitudes in T_1-weighted MR images [6], are the most prevalent contrast agents. In clinical MRI, such contrast agents are frequently used for assessing tissue perfusion. However, the application of contrast agents in NMR microscopy is relatively uncommon. Examples of such applications are characterizations of CA diffusion in hydrogels [7,8] and measurements of concentration maps of CA in animal cell bioreactor systems [9]. Here, we use Cu ions and the chelate Gd-DTPA as contrast agents for probing the permeability of microcapsules.

Microcapsules consisting of natural polysaccharide hydrogels such as alginates or pectinates are frequently used for the encapsulation and transportation of drugs and for the transplantation of cells [10–12]. The encapsulation protects the content of the capsules against outer influences like enzymes of the gastrointestinal tract and provides the possibility of controlled and site-specific release. If the capsules should be used for colon targeted delivery, they must posses a low permeability for the ingredient in the stomach, whereas they should have a high permeability or even dissolve in the colon. For achieving these properties, the pure hydrogel capsules can be modified by applying additional coatings like chitosan, poly-L-lysine or shellac [13–15].

The microcapsules studied here consist of the natural polysaccharide pectin which can be extracted from the cell walls of higher plants [16]. Low esterified pectins form three-dimensional ionotropic hydrogels with divalent cations. Here, we use this property to produce liquid filled spherical capsules with a membrane of calcium pectinate hydrogel. Since the permeability of these pure hydrogel capsules is too high for many applications [17], we coat them with shellac, a physiologically harmless and biodegradable resin secreted by the female lac bug (*kerria lacca*), which precipitates in acidic environments [18,19] and is commonly used as a coating material in pharmaceutical applications as well as in the food industry [20]. In previous studies, it was used to coat pectin matrix tablets which have recently been used for transporting

* Corresponding author.
E-mail address: stefan.henning@tu-dortmund.de (S. Henning).

1090-7807/$ - see front matter © 2012 Elsevier Inc. All rights reserved.
http://dx.doi.org/10.1016/j.jmr.2012.05.009

drugs to the colon [21] or as an additive to form pectinate-shellac composite capsules with improved mechanical stability [22].

In an earlier study, we showed how the application of an external shellac coating can be used to adjust the permeability of hydrogel capsules by combining magnetic resonance (MR) imaging with release measurements performed by UV/VIS spectroscopy [23]. In that study, two different experimental methods (NMR imaging and UV/VIS spectroscopy) were needed for determining diffusion coefficients of the capsule membranes. Here, we utilize contrast agent enhanced dynamic NMR microimaging to characterize the permeability with a single measurement technique. A serial acquisition of NMR images of capsules, which were placed into a CA solution, leads to time and permeability depending signals arising from the liquid capsule core. From these concentration profiles, we extract the diffusion coefficients by fitting a numerical solution of the diffusion process to the experimental data.

Dynamic NMR microscopy can not only be used for permeability measurements, but also to characterize the stability of the capsules in different chemical environments. When used for colon targeted delivery, the capsules must not release the encapsulated drug in the stomach and the small intestine, but in the colon. This property can be achieved if the capsules do not change their structure in the stomach and small intestine, whereas they dissolve in the colon. By performing NMR imaging of capsules in different solutions simulating gastrointestinal conditions, we investigate structural changes and dissolution processes under gastric, intestinal and colonic conditions.

2. Permeability measurements

The production of the capsules follows the technique described in [23]. Details are given in Appendix A and B.

2.1. Measurement of contrast agent diffusion

NMR microscopy offers the possibility to obtain a two dimensional image of the relaxation-time weighted spin-density of a slice through a sample by applying pulsed magnetic field gradients [1]. The higher static magnetic fields and the stronger pulsed magnetic field gradients (here ≈1 T/m) result in greatly enhanced spatial resolution of NMR microscopy compared to clinical MRI, thus allowing us to use it for characterizing microcapsules. We used a modified spin echo imaging sequence [24] for acquiring NMR images of the capsules on a 14 T Varian CMX Infinity Plus 600 spectrometer, which is equipped with a Resonance Research BFG-73/45–100 MK 2 gradient unit and a 5 mm inner diameter Bruker microimaging probe. Using this equipment, we achieve spatial resolution on the order of 10 μm.

Contrast agents (CA) are commonly used in medical MR imaging. Most of them are molecules including atoms with unpaired electrons with a long electronic relaxation time that enhance the relaxivity of surrounding molecules like water due to paramagnetic relaxation. Their contribution to the relaxation rate is proportional to their concentration. The application of such molecules as contrast agents in MR imaging relies on the opportunity to achieve contrast between regions of different relaxation times by adjusting the echo time (T_E) and repetition time (T_R). Contrast agents can be used for permeability measurements of microcapsules by placing them into a CA solution and consecutively acquiring NMR images. If the parameters in the pulse sequence are well chosen (i. e. repetition times ≈T_1), the NMR images show a significant contrast between regions of different CA concentrations. Thus, a serial acquisition of images allows us to measure the time-dependence of the concentration profile if the diffusivity of the CA molecules is low compared to the acquisition time. Here, we use the contrast agent Gd-DTPA, which is frequently used in medical imaging, and the ion Cu^{2+}. Using different molecules with different sizes offers the opportunity to determine molecular-size depending permeabilities.

For preparing the permeability measurement, a 5 mm outer diameter NMR tube was filled with an aqueous solution of the contrast agent with initial concentration c_0 (1.83 mmol/l Gd-DTPA or 7.44 mmol/l Cu^{2+}). The CA solution was adjusted to an acidic pH of 6 by adding calciumchloride in order to assure that the capsules do not dissolve while the permeability measurement takes place. The pH value could not be set to a lower value because the stability of the Gd-DTPA complex decreases dramatically at more acidic pH values. The NMR tube also contained a susceptibility plug at the bottom. This plug has a small drilling in its center to fix the position of the capsule. It consists of polyetherimide, which has a magnetic susceptibility similar to that of water.

In order to start the experiment, a microcapsule with a diameter of 1–2 mm was transferred from an aqueous storage solution (including 0.5 %wt $CaCl_2$, pH = 6) into the NMR tube. As the capsule came into contact with the CA solution, the CA molecules started to diffuse into the capsule. The NMR tube was quickly inserted into the probe and the magnet of the NMR spectrometer. Then, an image of a vertical plane through the sample was acquired to determine the vertical position of the capsule. After that, the actual measurement was started by successive acquisition of images in a horizontal plane through the center of the capsule. The time between the first contact of the capsule with the contrast agent solution in the tube and the initialization of the acquisition of the NMR images used for the diffusion visualization was measured and taken into account in the analysis described in Section 2.3. For all measurements, this time delay was about 90 s. After the acquisition of one image, which took 1.3 min, the next image acquisition was directly initiated. For one permeability measurement, about 100–1000 images were acquired, depending on the time until equilibrium between concentration inside and outside of the capsules was achieved.

The images were acquired with a FOV (field of view) of (6 × 6) mm^2 and a slice thickness of approximately 150 μm. A four steps phase cycle was used for improving the signal to noise ratio and suppressing imaging artifacts. The echo time was set to 20 ms, whereas the repetition time was adjusted to 150 ms. This short time compared to T_1 of pure water (≈2 s) yielded in a contrast between regions of high and low CA concentrations since in high concentrated regions T_1 is approximately 100 ms. Due to this contrast, the diffusion of the contrast agent into the capsule could be well visualized. The acquisition time for one image was ≈1 min.

Due to technical limitations, all experiments were performed at a temperature of 10 °C.

For enhancing the image quality, we processed the k-space data by applying a $\sin^2$ apodization and a zero filling in the phase encoding and frequency encoding directions before performing a two dimensional Fourier transformation. The pixel size of the resulting images was (11.5 × 11.5) μm^2.

2.2. Calculating the concentration of contrast agents

For a voxel in an NMR image acquired with a spin echo sequence, the signal amplitude is given by [25]

$$S = S_0 \cdot e^{-\frac{T_E}{T_2}} \cdot \left(1 - 2e^{-\left(\frac{T_R}{T_1} - \frac{T_E}{2T_1}\right)} + e^{-\frac{T_R}{T_1}}\right). \quad (1)$$

In this equation, T_E and T_R represent the echo time and the repetition time of the sequence, whereas T_1 and T_2 are the longitudinal and transversal relaxation times.

For liquid solutions of paramagnetic molecules a linear relation between the relaxation rates $R_{1,2} = T_{1,2}^{-1}$ and their concentrations c can be assumed:

$$R_{1,2}(c) = k_{1,2} \cdot c + R_{1,2}(0). \tag{2}$$

In order to obtain these functions for the contrast agents used in our experiments, we measured the relaxation times of differently concentrated solutions before the permeability experiments were performed. With the help of Eq. (1) the parameters T_E and T_R in the imaging sequence and the value of c_0 were chosen by considering that the slope of the signal function should be high, that signal amplitude is maximized and that the used c_0 is below the maximum position of the signal function. These considerations yielded a good contrast between regions of different CA concentrations, a high signal to noise ratio in the images and a distinct allocation of concentrations to signal amplitudes.

For each acquired NMR image a contour tracing algorithm was used to find contour lines that separate regions of different signal amplitudes. With these contour lines, we could assign all voxels to the different areas of the sample (air and tube wall (noise), contrast agent solution, capsule membrane and liquid core of the capsule). The contour lines also allowed for automatic determination of the center and diameter of the capsule and its membrane thickness, which is needed for the fitting procedure described in the next chapter.

The parameter S_0 in Eq. (1) can be obtained from the amplitude $S_{CA-sol.}$ of the voxels corresponding to the contrast agent solution with concentration $\approx c_0$ in the first acquired image:

$$S_0 = \frac{\langle S_{CA-sol.}\rangle_{1\text{stimage}} - \langle \text{noise}\rangle_{1\text{st image}}}{e^{-T_E/T_2(c_0)}\left(1 - 2e^{-\left(\frac{T_R}{T_1(c_0)} - \frac{T_E}{2T_1(c_0)}\right)} + e^{-\frac{T_R}{T_1(c_0)}}\right)}, \tag{3}$$

where $\langle \text{noise}\rangle_{1\text{st image}}$ represents the average amplitude of the pixels in the wall and air regions. Using Eq. (3) with (1) allows for calculating the contrast agent concentration in each voxel of the image. In addition to the concentration calculation, the distance of each voxel in the liquid core to the center of the capsule was also calculated, leading to time and distance dependent concentration profiles $c_{exp}(r, t)$.

2.3. Numerical simulation of diffusion and fitting of diffusion coefficients

The basis for a theoretical description of the diffusion process is Fick's 2nd law. For systems with a radial symmetry, it can be written as

$$\frac{\partial c}{\partial t} = D\left(\frac{\partial^2 c}{\partial r^2} + \frac{2}{r}\frac{\partial c}{\partial r}\right), \tag{4}$$

where r is the distance to the center of symmetry. This partial differential equation describes how the concentration c of a molecule with diffusivity D changes with time t and place r under a concentration gradient.

Considering the diffusion of a solute into a sphere in a solution bath with volume V, Crank derived an analytical solution of Eq. (4) for describing the concentration within the sphere depending on time and diffusion coefficient [26]. However, this solution is only applicable if the bath is well stirred. So for our experiment, where the capsules are in a bath that is not in motion, Crank's solution can't be used. Therefore, we solved Eq. (4) numerically by using the MATLAB function *pdepe* with the initial conditions

$$\begin{aligned} &c(r = 0 \ldots r_{out}, t = 0) = 0 \\ &c(r = r_{out} \ldots r_{bath}, t = 0) = c_0, \end{aligned} \tag{5}$$

where r_{out} is the outer radius of the investigated capsule (radius of liquid core (r_{in})+membrane thickness) and r_{bath} is the radius which a spherical bath would have with a volume equal to the volume of the solution in the NMR tube. We used a coordinate system which has its origin ($r = 0$) in the center of the capsule. Choosing the boundary conditions as

$$\left.\frac{\partial c}{\partial r}\right|_{r=0} = \left.\frac{\partial c}{\partial r}\right|_{r=r_{bath}} = 0 \tag{6}$$

and assuming a spatially variable diffusion constant

$$\begin{aligned} &D(r = 0 \ldots r_{in}) = D(r = r_{out} \ldots r_{bath}) = D_{free} \\ &D(r = r_{in} \ldots r_{out}) = D_{membrane}, \end{aligned} \tag{7}$$

we obtained the two dimensional concentration profile $c_{num}(r,t)$ depending on the size of the capsule and the diffusion coefficients in the capsule membrane ($D_{membrane}$) and in water (D_{free}). This numerical solution was used in a least square fitting procedure to obtain $D_{membrane}$ and D_{free} from the measured concentrations.

The correctness of the numerical solution was tested by comparing Crank's analytical solution to a numerical solution in which the diffusivity in the bath was adjusted to a very high value, simulating stirring. Both methods yielded the same solution.

2.4. Results and discussion

Fig. 1 shows NMR images of two exemplary measurements which were acquired while the CA was diffusing into uncoated (a) and coated (b) capsules. In the first images, which correspond to a diffusion time of 2 min, the signal arising from the capsule core is very weak, indicating low CA concentration and therefore long relaxation times. As time increases, the contrast agent diffuses into the capsule and leads to stronger signals from the liquid core. In the images where the signal from the core is strong enough, the capsule membrane, the core and the surrounding solution are well distinguished, because the signal from the membrane is very low. The signal reduction in the membrane area results from the short transverse relaxation time. In a previous study, we used microimaging for visualizing the different layers of the membrane [23]. In the present images, the different layers of the membrane cannot easily be identified, since the measurement parameters were optimized for diffusion studies, rather than precise geometrical measurements.

In order to calculate the concentration of the contrast agent in each voxel, we measured T_1 and T_2 for solutions with different concentrations and performed a linear least squares fit to obtain the parameters $k_{1,2}$ and $R_{1,2}(0)$ in Eq. (2). Table 1 summarizes the results of the fitting procedure. It is obvious that the molar relaxivity is much higher for Gd-DTPA than for Cu^{2+} which is a consequence of the high magnetic moment of the gadolinium ion.

Fig. 2a shows the CA concentration inside the capsule as a function of time and distance to the center of the capsule. In order to obtain a radial dependence of the concentrations, we calculated the mean value of the signal amplitudes averaged over a range of distances to the capsule center. We then used Eqs. (1) and (2) to convert the signal amplitudes into concentrations. For short diffusion times, the overall concentration in the capsule is very low, but a significant concentration gradient from the center of the capsule to the membrane can be recognized. For longer diffusion times, this concentration gradient decreases, since the diffusivity of the CA is higher in the liquid core than in the capsule membrane. For long times, the concentration in the capsule approaches the equilibrium value of the solution outside of the capsule. This equilibrium concentration value is roughly the same as the initial concentration of the CA solution since the solution volume is about 1000 times the capsule volume.

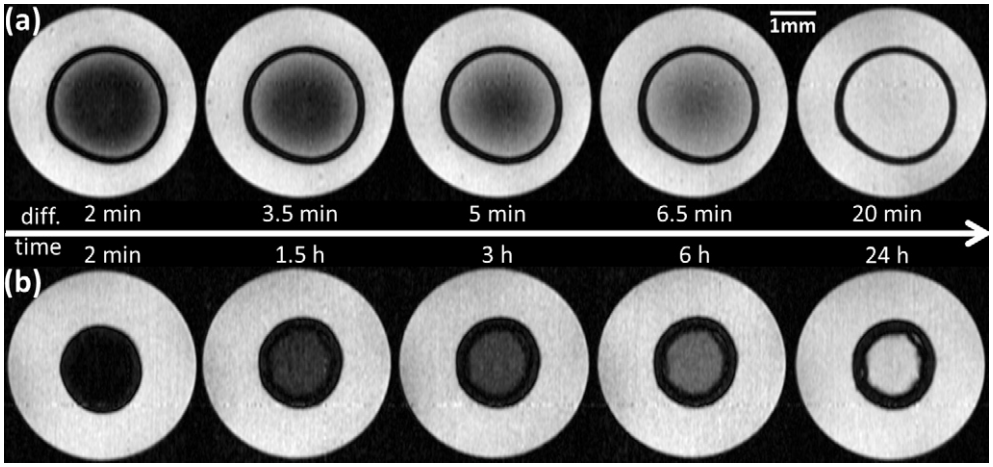

Fig. 1. NMR images which visualize how the contrast agent Gd-DTPA diffuses into an uncoated pectinate microcapsule (a) and into a shellac coated pectinate microcapsule (b) leading to time dependent signal amplitudes within the capsule cores.

Table 1
Fitted parameters describing the linear dependence of the relaxation rates on the concentration.

Contrast agent	k_1 (l/s mmol)	$R_1(0)$ (s^{-1})	k_2 (l/s mmol)	$R_2(0)$ (s^{-1})
Gd-DTPA	4.94	0.03	6.28	1.2
Cu^{2+}	0.94	0.2	1.28	1.0

From a numerical solution of Eq. (4), we can determine diffusion coefficients for the contrast agent in the solution and liquid capsule core (D_{free}) and in the membrane (D_{mem}). Fig. 2b shows the concentration profile, which was obtained by a least squares fit to the experimental data plotted in Fig. 2a, using D_{free} and D_{mem} as adjustable parameters. A two-dimensional comparison between the simulated and experimental data is given in Appendix C.

The obtained diffusion coefficients of Gd-DTPA and Cu^{2+} in different membrane compositions are summarized in Table 2. We performed three measurements for each combination of contrast agent and capsule type. Regarding the uncoated pectinate capsules, all repeated measurements yielded similar results. The diffusion coefficients of Cu^{2+} and Gd-DTPA in the membrane are reduced by a factor of six to seven in comparison to the free diffusion in the capsule core and outer solution. Differences of D_{free} between the contrast agents are a result of different molecular sizes. As

Table 2
Diffusion coefficients of contrast agents in capsule membranes and water obtained by fitting a numerical simulation to the experimental data. Estimated accuracy: 15% for D_{mem} and 20% for D_{free}. The different numerical values for the diffusion coefficients correspond to different capsules and indicate the range of observed values.

Contrast agent	Capsule type	D_{mem} $\left(10^{-11}\ m^2/s\right)$	D_{free} $\left(10^{-11}\ m^2/s\right)$
Gd-DTPA	Uncoated	5	30
Cu^{2+}	Uncoated	11	80
Gd-DTPA	Coated	5/0.06/≈0	30/30/n.a.
Cu^{2+}	Coated	6/0.02	80/80

expected, the fitted values of D_{free} are the same for coated and uncoated capsules. Concerning the fitted diffusion coefficients in shellac coated membranes, we obtained different results for each repeated measurement. The diffusion coefficient in the membrane varies over a large range from values similar to that of uncoated pectinate membranes and nearly zero. In the latter case, we could not observe any changes of the concentration inside the capsule over a period of about 4 weeks.

In a previous study, we characterized the permeability of similar capsules for anthocyanins $\left(D_{free} = 7.4 \times 10^{-11}\ m^2/s\right)$ with UV/VIS spectroscopy [23]. These measurements resulted in diffusion

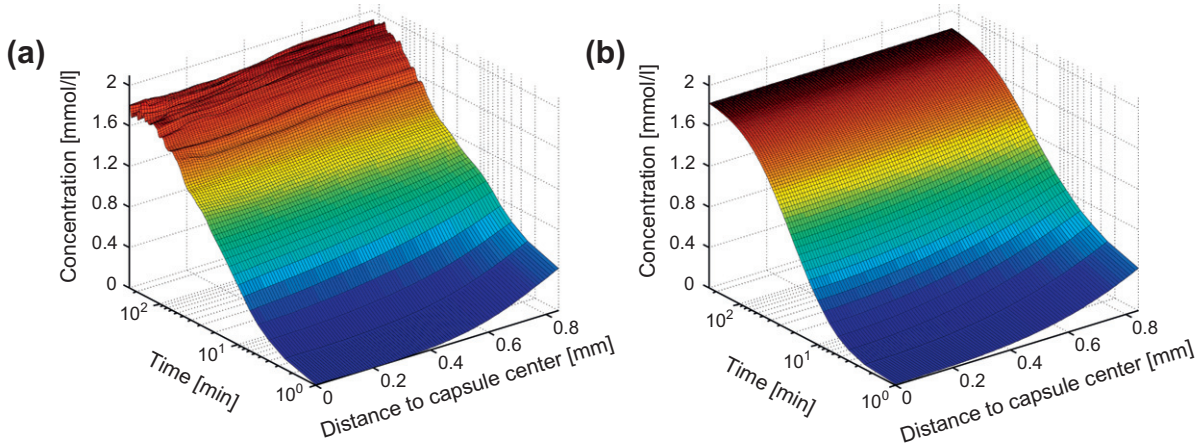

Fig. 2. Time dependent concentration profiles of the contrast agent Gd-DTPA in an uncoated pectinate capsule. The left-hand data were calculated from measured NMR images and the right-hand data were calculated from a numerical solution of the diffusion equation.

coefficients of $D_m = 7 \times 10^{-11}$ m^2/s for uncoated capsules and $D_m = 1 \times 10^{-11}$ m^2/s for coated capsules, respectively. In contrast to the experiments described here, the former diffusion measurements were performed with many capsules simultaneously, leading to mean diffusion coefficients for all capsules. Taking into account that the diffusion coefficients fitted in this earlier study are effective coefficients for the diffusion in the membrane and in the capsule core, D_{mem} of anthocyanins and Gd-DTPA in uncoated pectinate membranes are nearly the same, although D_{free} of Gd-DTPA is more than four times higher than D_{free} of anthocyanins. This discrepancy may be explained by electrostatic interactions of the positively charged anthocyanin molecules with negative charges in the pectinate polysaccharide.

The observation of widely spread membrane permeabilities of coated capsules is a hint for a suboptimal preparation process that leads to coatings with different qualities. In order to explain the variable permeabilities of coated capsules, we acquired three dimensional NMR images of two capsules which showed a strong difference in their permeability. In the 3D image (Fig. 3) of the high permeability capsule we could see that the shellac was cracked at some places leading to holes in the coating layer. In contrast to that, the surface of the capsule with low permeability did not show any damage. This observation indicates that the shellac coating itself is not permeable for the contrast agents that we tested, but that the permeabilities of coated capsules are a result of defects in the coating layer. Optimizing the preparation process should yield capsules that show no permeability for molecules which are comparable to the used contrast agents and environmental conditions in our experiments.

For the applicability of the capsules as oral drug carriers, it is important that the permeability is also low at physiological temperatures. Since all diffusion measurements described before were performed at a temperature of 10 °C due to experimental restrictions, we performed an additional permeability measurements at 37 °C of the capsule that showed no permeability for Gd-DTPA. Again, the capsule showed no permeability for the contrast agent.

3. Stability measurements

3.1. Visualization of capsule stability and dissolution

Besides the permeabilities of the studied microcapsules, their behavior under gastrointestinal conditions is also vitally important. We characterized that in vitro by consecutively acquiring MR images in solutions adjusted to gastric, intestinal and colonic conditions. For the acquisition, we either used the same spin echo imaging sequence as used for the permeability measurements or a fast low angle shot (FLASH) imaging sequence [27], depending on the rate at which structural changes of the capsule appeared.

Fig. 3. Three dimensional surface reconstruction of a high permeability capsule obtained by combining multiple two dimensional NMR images of different slices. The crack in the outer shellac layer leads to a high permeability.

The solutions that were used for simulating gastrointestinal (GI) conditions were adjusted to pH-values similar to the pH-values of the stomach (pH = 1.2), the small intestine (pH = 6.8) and the colon (pH = 7.4) according to typical GI formulations [28]. In order to evaluate the applicability of the capsules for colonic delivery, images were acquired while the capsules remained 2 h in the stomach simulation solution and 3 h in the small intestine solution, which are typical transit times of drug carriers in the human GI tract. Image acquisition of the capsules remaining in the colonic solution was performed until capsules were completely dissolved.

The stability measurement was initiated by transferring a capsule from a storage solution into an NMR tube containing stomach simulation solution. After a quick insertion of the sample into the NMR probe and magnet, seven images of a horizontal plane through the center of the capsule were acquired while the capsule was influenced by the stomach solution. Afterwards, the NMR tube was retrieved from the probe and the simulation solution was exchanged. In order to assure that the pH-value of the solution was not influenced by this exchange, the NMR tube and the capsules were washed out with the following small intestine solution, before the final solution was applied. Then the procedure was repeated as described above, until after 10 measurements in the small intestine solution, the chemical environment was changed to the colon solution. Under these conditions, images were acquired until the capsule was completely dissolved. The whole measurement was performed at a temperature of 37 °C.

Images of the capsules in the stomach and small intestine solution were acquired with the same imaging sequence and almost the same parameters as used in the permeability measurements. In contrast to the T_1 weighted images in the permeability experiments, we now used T_2 weighted images with repetition times adjusted to 2 s and echo times adjusted to 40 ms (stomach solution) or 100 ms (small intestine solution). Using these parameters, the acquisition of one image took 17 min. For investigating the capsules in colon solution, we used two different pulse sequences for image acquisition. If structural changes of the capsules appeared slowly, image acquisition was performed in the same way as performed for the small intestine solution. If structural changes of the capsule were fast, the time needed for image acquisition had to be significantly reduced. Since T_1 of the colon solution was about 2 s, we could not decrease acquisition time by adjusting the repetition time to much shorter values. Hence, we used a FLASH imaging sequence which allowed us to reduce the acquisition time to 1 min. That short time was achieved by using a flip angle of 18°, T_E = 22 ms and T_R = 110 ms.

3.2. Results and discussion

Images of shellac coated pectinate capsules with different coatings (for details of the coating process see Appendix A) were obtained with a FLASH and a spin echo imaging sequence under simulated GI conditions. None of the capsules showed any changes in appearance in acidic solutions simulating the stomach (pH = 1.2) and small intestine (pH = 6.8), whereas they showed remarkable structural changes in basic solutions simulating the colon (pH = 7.4). Fig. 4 shows a subset of consecutively acquired spin echo NMR images demonstrating the behavior of two capsules under simulated GI conditions.

The images taken under gastric and intestinal conditions do not depict any structural changes of the capsules. Due to a compromise between image quality and acquisition time, the pectinate and

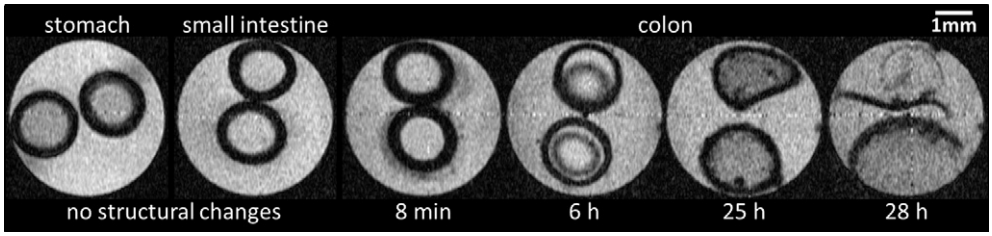

Fig. 4. Exemplary NMR images of coated pectinate microcapsules (10 min coating time and 5% PVP concentration) acquired under simulated gastrointestinal conditions demonstrating that the capsules do not underly structural changes in the stomach and small intestine solution, but dissolve in colon solution.

shellac layers cannot be distinguished very well in these images. The third to sixth image of Fig. 4 show how the capsules behave under colonic conditions. In these basic pH conditions, we can observe a tightening and dissolving of the inner pectinate membrane. In contrast to our observation, pectinate normally should swell under basic conditions [29]. We assume that the interaction of different competing chemical processes, e.g. hydrolytic scission of the polysaccharide chains and the complexation of cross-linking calcium ions by the phosphate buffer in colon solution, causes the pectinate hydrogel to tighten and to dissolve. Some time after the dissolution of the inner pectinate membrane, also the shellac membrane first breaks and then dissolves due to a high solubility of shellac in basic environments.

In the measurement depicted in Fig. 4, which was performed with a capsule coated with a coating time of 10 min and a PVP concentration of 5%, about 28 h elapsed until the capsule dissolved. This is much too long for an adequate colonic delivery system. Thus, we varied coating times and concentrations of PVP used in the capsule preparation. The resulting dissolution times are shown in Table 3. Higher concentrations of PVP and shorter coating times lead to significant reduction of durations needed for the capsules to dissolve.

Fig. 5 demonstrates the observed dissolution process of capsules coated for 10 min with a PVP concentration of 10%. Here the first image shows cracks in the shellac coating and the capsules start to dissolve already in the first two images. The dissolution of the pectinate membrane also proceeded faster possibly because the cracks in the shellac layer lead to an earlier exposure to the basic environment. For this measurement, we could observe that the capsules dissolved completely in about 3 h. Further reduction of the dissolution time down to about 1 h could be achieved by decreasing the coating time. Images of those capsules were acquired with a FLASH sequence since this technique allowed us to observe the dissolution process with a time resolution of 1 min. We created a video of the FLASH images which illustrates the dissolution process. This video can be found in the digital attachment.

4. Conclusion

NMR microimaging has proved to be an excellent tool for investigating the permeability and stability of small drug carriers. We obtained diffusion coefficients of contrast agents in the membranes of uncoated and shellac coated pectinate microcapsules and observed that the coating strongly decreases the permeability of their membrane.

Table 3
Dissolution times depending on the capsule preparation process.

Coating time (min)	PVP concentration (%)	Colonic dissolution time (h)
10	5	28
10	10	3
5	10	1
3	10	1

In contrast to other methods usually applied for measuring permeabilities of drug carriers like UV/Vis spectroscopy, dynamic NMR imaging has some advantages. Usual methods need a large amount of drug carriers, whereas our new method described here can be performed with one single capsule. This allows for a better understanding of the mechanisms responsible for the specific permeability. Concerning the quantitative analysis of permeability measurements, which means to obtain diffusion constants, usual methods like UV/Vis spectroscopy need additional measurements of capsule properties like the diameter or the membrane thickness. When using dynamic NMR microscopy for obtaining diffusion coefficients, only one single measurement is necessary.

In the example given here, we used paramagnetic contrast agents to study the permeability of the capsule membrane. Clearly, the retention times for different molecules depend on various parameters, such as molecular weight and charge. Measuring the permeability is significantly easier if the molecule is paramagnetic. If retention times are needed for specific molecules, such as drugs, which are diamagnetic, it may be possible to use analogues that are paramagnetic or to attach spin labels to them.

In addition to the permeability measurements, we also studied the stability and monitored the dissolution process of microcapsules in different chemical environments to evaluate their applicability for specific purposes. We showed that shellac coated capsules do not undergo structural changes under gastric and intestinal conditions. However, MR images taken of the capsules under colonic conditions reveal that the capsules dissolve on a timescale of 1–28 h, depending on the capsule preparation process.

As the measurements in our studies show, shellac coated pectinate capsules provide all the properties required from a system for colonic drug delivery.

Appendix A. Materials

The used amidated pectin (Pectin amid AU-L 027/09) was provided by Herbstreith & Fox KG, Germany. The aqueous ammoniacal shellac solution (SSB Aquagold, 25% solid content, pH $\approx$ 7.5) for the external coating was provided by SSB Stroever Schellack Bremen, Germany. $CaCl_2{\cdot}2H_2O$ and anhydrous glycerol ($\geqslant$99%) were purchased from Merck Chemicals, Germany. The contrast agents $CuSO_4{\cdot}6H_2O$ and Diethylenetriaminepentaacetic acid gadolinium (III) dihydrogen salt hydrate (Gd-DTPA) were purchased from Sigma–Aldrich, Germany. Polyvinylpyrrolidone (PVP) used as softening agent was purchased from Harke Pharma, Germany. All chemicals were used without further purification.

Appendix B. Capsule preparation

Calcium pectinate capsules filled with a liquid core were prepared by extrusion in a simple one step process. For the preparation of all capsule types an aqueous amidated pectin solution of 0.8 %wt was used. The cross-linking solution consists of calcium-chloride dissolved in double distilled water. Furthermore, an

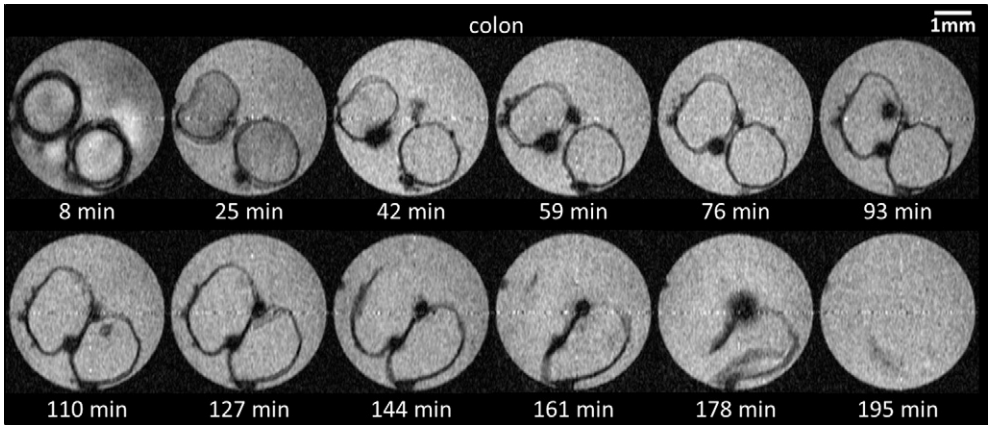

Fig. 5. Temporal evolution of NMR images from microcapsules (10 min coating time and 10% PVP concentration) in colon simulating solution.

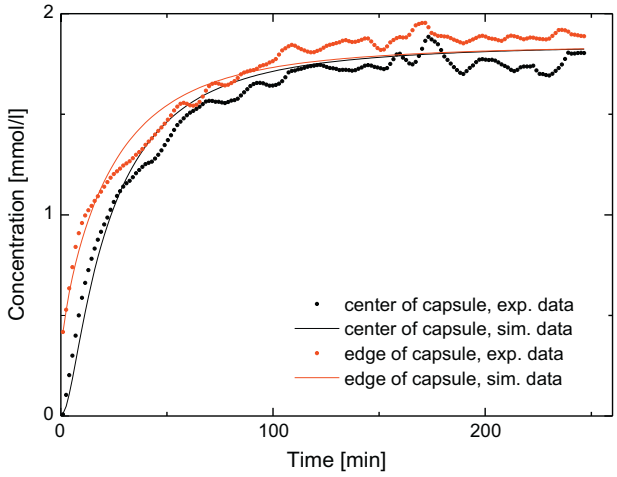

Fig. C.6. Simulated and measured concentrations of paramagnetic probe molecules as a function of time at the edge and the center of the capsule for the measurement shown in Fig. 2.

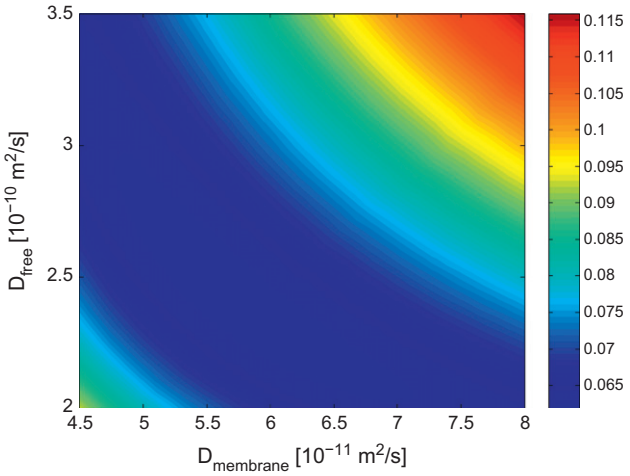

Fig. C.7. RMS deviation (in mmol/l) as a function of $D_{membrane}$ and D_{free} for the measurement shown in Fig. 2. The minimum RMS deviation of ≈0.06 mmol/l is found at $D_{membrane} \approx 5.5 \times 10^{-11}$ m^2/s and $D_{free} \approx 2.5 \times 10^{-10}$ m^2/s.

aqueous ammoniacal shellac solution was used to create an external coating around the calcium pectinate capsules.

In detail, for the preparation of the cross-linking solution, 2.0 %wt $CaCl_2 \cdot 2H_2O$ salt was dissolved in 100 ml of double distilled water. After that, the supernatant solution was diluted with the same amount of anhydrous glycerol, which was added to improve the mechanical properties as well as the density for facilitating the dropping in. The resulting cross-linking solution contained 50 %vol glycerol and 1.0 %wt calciumchloride. A pH value of 3 was adjusted by adding some drops of hydrochloric acid.

In the capsule production process, firstly the cross-linking solution was added drop-wise by means of a high-precision syringe into a cylindrical glass filled with 30 ml of an aqueous 0.8 %wt pectin solution. A capsule membrane was formed instantly around each droplet once the two liquids came into contact. Because the calcium cation has a smaller size than the polymer molecules, it can diffuse into the pectin solution and this leads to cross-linking processes in which intermolecular cross-links are formed between the divalent calcium ions and the negatively charged carboxyl groups of the amidated pectin molecules [30]. Induced by these diffusion processes the gel membrane grows along the flux direction of the calcium ions [31]. In order to avoid the aggregation of the prepared capsules, the pectin solution was constantly moved by a magnetic stirrer. A dropping height of 2 cm was used to ensure that nearly spherical capsules were formed. Experimental tests showed that for larger distances, the drops were destroyed when they came into contact with the surface of the pectin solution. If the dropping height was reduced to less than 2 cm, the resulting capsules showed distortion wedges. After gelation times of 30 s, the capsules were separated, filtered and washed with double distilled water.

Two additional steps were necessary to apply an external shellac coating. Firstly, after isolating the capsules they were transferred into an aqueous solution containing 2.0 %wt $CaCl_2 \cdot 2H_2O$, with the aim of stabilizing the gel membranes and completing the polymerization process [32]. This calcium chloride solution was adjusted to a pH value of 1 by adding hydrochloric acid. To achieve a homogeneous pH-value throughout the capsule by diffusion of the hydrogen ions, we left them in the acidic medium for 5 min.

In the last step, after the capsule separation and filtration, the capsules were transferred into the coating solution, containing 20 %wt aqueous ammoniacal shellac solution and 5.0–10.0 %wt anhydrous glycerol (or polyvinylpyrrolidone for stability measurements) used as softening agent, to apply a shellac coating around the calcium pectinate capsules. The diffusion of the positively charged hydrogen ions from the capsules induces the precipitation of the shellac and therefore the formation of a shellac coating. After

a residence time of 10 min (3, 5 or 10 min for stability measurements) in the coating solution, the capsules were separated, filtered, washed with double distilled water and transferred into a 2.0 %wt $CaCl_2 \cdot 2H_2O$ solution adjusted to a pH value of 1 for storage.

The produced liquid-filled and shellac coated pectinate capsules exhibit diameters in the range of 1–2 mm and entire membrane thicknesses in the range of 100 μm up to 300 μm.

Appendix C. Quantitative comparison of measured and simulated concentrations

In order to compare the experimental concentration profile with the fitted concentration profile obtained by numerical simulations, we show the experimental and simulated concentrations as a function of time at two different places inside the capsule (edge of liquid core and center). For short times the deviations between simulated and experimental curves are quite small. At longer times, the experimental curves fluctuate, which results in bigger deviations between theoretical and experimental curves. These oscillations can be traced to Eq. (1) which was used to calculate the concentrations. For high concentrations, the derivative $\frac{\partial S}{\partial c}$ becomes smaller and constant experimental noise leads to larger errors in the concentration (see Fig. C.6).

Fig. C.7 shows the root mean square (rms) deviation between the simulated and experimental concentrations as a function of the diffusion coefficients used in the numerical solution of the diffusion equation. The optimal values for the diffusion coefficients correspond to the minimum of this function. The experimental uncertainties are 15% and 20% for D_{mem} and D_{free}, respectively.

Appendix D. Supplementary data

Supplementary data associated with this article can be found, in the online version, at http://dx.doi.org/10.1016/j.jmr.2012.05.009.

References

[1] P.T. Callaghan, Principles of Nuclear Magnetic Resonance Microscopy, Oxford University Press, Oxford, 1993.
[2] B. Blümich, W. Kuhn (Eds.), Magnetic Resonance Microscopy, VCH, 1992.
[3] E.O. Stejskal, J.E. Tanner, Spin diffusion measurements: spin echoes in the presence of a time-dependent field gradient, Journal of Chemical Physics 42 (1965) 288–292.
[4] P.T. Callaghan, Y. Xia, Velocity and diffusion imaging in dynamic NMR microscopy, Journal of Magnetic Resonance 91 (1991) 326–352.
[5] A. Jackson, D. Buckley, G. Parker (Eds.), Dynamic Contrast-Enhanced Magnetic Resonance Imaging in Oncology, Springer, Berlin, 2005.
[6] J.E. Kirsch, Basic principles of magnetic resonance contrast agents, Topics in Magnetic Resonance Imaging 3 (1991) 1–18.
[7] K. Potter, E.W. McFarland, Ion transport studies in calcium alginate gels by magnetic resonance microscopy, Solid State Nuclear Magnetic Resonance 6 (1996) 323–331.
[8] M.J. Gordon, K.C. Chu, A. Margaritis, A.J. Martin, C.R. Ethier, B.K. Rutt, Measurement of Gd-DTPA diffusion through PVA hydrogel using a novel magnetic resonance imaging method, Biotechnology and Bioengineering 65 (1999) 459–467.
[9] P.E. Thelwall, A.A. Neves, K.M. Brindle, Measurement of bioreactor perfusion using dynamic contrast agent-enhanced magnetic resonance imaging, Biotechnology and Bioengineering 75 (2001) 682–690.
[10] P. de Vos, M.M. Faas, B. Strand, R. Calafiore, Alginate-based microcapsules for immunoisolation of pancreatic islets, Biomaterials 27 (2006) 5603–5617.
[11] C.P. Champagne, P. Fustier, Microencapsulation for the improved delivery of bioactive compounds into foods, Current Opinion in Biotechnology 18 (2007) 184–190.
[12] E. Murano, Use of natural polysaccharides in the microencapsulation techniques, Journal of Applied Ichthyology 14 (1998) 245–249.
[13] V. Ravi, Siddaramaiah, T.M. Pramod Kumar, Influence of natural polymer coating on novel colon targeting drug delivery system, Journal of Materials Science. Materials in Medicine 19 (2008) 2131–2136.
[14] S.H. Chiou, W.T. Wu, Y.Y. Huang, T.W. Chung, Effects of the characteristics of chitosan on controlling drug release of chitosan coated PLLA microspheres, Journal of Microencapsulation 18 (2001) 613–625.
[15] F. Lim, A.M. Sun, Microencapsulated islets as bioartificial endocrine pancreas, Science 210 (1980) 908–910.
[16] P. Sriamornsak, Chemistry of pectin and its pharmaceutical uses: a review, Silpakorn University International Journal 3 (2003) 206–228.
[17] D.S. Ferreira, A.F. Faria, C.R.F. Grosso, A.Z. Mercadante, Encapsulation of blackberry anthocyanins by thermal gelation of curdlan, Journal of the Brazilian Chemical Society 20 (2009) 1908–1915.
[18] M. Penning, Aqueous Shellac Solutions for Controlled Release Coatings, in: D.R. Karsa, R.A. Stephenson (Eds.), Chemical Aspects of Drug Delivery Systems, RSC, Cambridge, 1996, pp. 146–154.
[19] D. Phan The, F. Debeaufort, D. Luu, A. Voilley, Moisture barrier, wetting and mechanical properties of shellac/agar or shellac/cassava starch bilayer biomembrane for food applications, Journal of Membrane Science 325 (2008) 277–283.
[20] R.-K. Chang, G. Iturrioz, C.-W. Luo, Preparation and evaluation of shellac pseudolatex as an aqueous enteric coating system for pellets, International Journal of Pharmaceutics 60 (1990) 171–173.
[21] V. Ravi, T. Kumar, Siddaramaiah, Novel colon targeted drug delivery system using natural polymers, Indian Journal of Pharmaceutical Sciences 70 (2008) 111–113.
[22] S. Leick, M. Kott, P. Degen, S. Henning, T. Päsler, D. Suter, H. Rehage, Mechanical properties of liquid-filled shellac composite capsules, Physical Chemistry Chemical Physics 13 (2011) 2765–2773.
[23] S. Henning, S. Leick, M. Kott, H. Rehage, D. Suter, Sealing liquid-filled pectinate capsules with a shellac coating, Journal of Microencapsulation (2011).
[24] E.W. Hsu, J.S. Schoeniger, R. Bowtell, N.R. Aiken, A. Horsman, S.J. Blackband, A modified imaging sequence for accurate T2 measurements using NMR microscopy, Journal of Magnetic Resonance, Series B 109 (1995) 66–69.
[25] R. Graumann, A. Oppelt, E. Stetter, Multiple-spin-echo imaging with a 2D Fourier method, Magnetic Resonance in Medicine 3 (1986) 707–721.
[26] J. Crank, The Mathematics of Diffusion, Oxford University Press, Oxford, 1979.
[27] A. Haase, J. Frahm, D. Matthaei, W. Hänicke, K.-D. Merboldt, FLASH imaging: rapid NMR imaging using low flip-angle pulses, Journal of Magnetic Resonance 67 (1986) 258–266.
[28] A.K. Anal, H. Singh, Recent advances in microencapsulation of probiotics for industrial applications and targeted delivery, Trends in Food Science & Technology 18 (2007) 240–251.
[29] S.T. Moe, G. Skjaak-Braek, A. Elgsaeter, O. Smidsroed, Swelling of covalently crosslinked alginate gels: influence of ionic solutes and nonpolar solvents, Macromolecules 26 (1993) 3589–3597.
[30] P. Sriamornsak, J. Nunthanid, Calcium pectinate gel beads for controlled release drug delivery: I. Preparation and in vitro release studies, International Journal of Pharmaceutics 160 (1998) 207–212.
[31] A. Blandino, M. Macias, D. Cantero, Formation of calcium alginate gel capsules: influence of sodium alginate and $CaCl_2$ concentration on gelation kinetics, Journal of Bioscience and Bioengineering 88 (1999) 686–689.
[32] Y. Chai, L.-H. Mei, D.-Q. Lin, S.-J. Yao, Diffusion coefficients in intrahollow calcium alginate microcapsules, Journal of Chemical & Engineering Data 49 (2004) 475–478.